Pseudospectral time-dependent density functional theory

Chaehyuk Ko, David K. Malick, Dale A. Braden, Richard A. Friesner, and Todd J. Martínez'

Citation: The Journal of Chemical Physics **128**, 104103 (2008); doi: 10.1063/1.2834222
View online: http://dx.doi.org/10.1063/1.2834222
View Table of Contents: http://aip.scitation.org/toc/jcp/128/10
Published by the American Institute of Physics

Pseudospectral time-dependent density functional theory

Chaehyuk Ko,[1] David K. Malick,[1] Dale A. Braden,[2] Richard A. Friesner,[3] and Todd J. Martínez[1,a)]
[1]*Department of Chemistry and The Beckman Institute, University of Illinois, Urbana, Illinois 61801, USA*
[2]*Schrodinger, LLC, Portland, Oregon 97201, USA*
[3]*Department of Chemistry, Columbia University, New York, New York 10027, USA*

(Received 7 November 2007; accepted 18 December 2007; published online 11 March 2008)

Time-dependent density functional theory (TDDFT) is implemented within the Tamm-Dancoff approximation (TDA) using a pseudospectral approach to evaluate two-electron repulsion integrals. The pseudospectral approximation uses a split representation with both spectral basis functions and a physical space grid to achieve a reduction in the scaling behavior of electronic structure methods. We demonstrate here that exceptionally sparse grids may be used in the excitation energy calculation, following earlier work employing the pseudospectral approximation for determining correlation energies in wavefunction-based methods with similar conclusions. The pseudospectral TDA-TDDFT method is shown to be up to ten times faster than a conventional algorithm for hybrid functionals without sacrificing chemical accuracy. © *2008 American Institute of Physics*.
[DOI: 10.1063/1.2834222]

INTRODUCTION

Density functional theory[1] (DFT) is now well established as one of the most efficient methods for computing electronic ground state properties. The description of excited state properties has required further development, since the exchange-correlation functional for excited states is not universal. Several methods have been advanced to extend the domain of applicability to electronic excited states, with the most promising being time-dependent density functional theory[2–5] (TDDFT). TDDFT is based on the Runge–Gross theorem,[6] which posits a one-to-one correspondence between the time-dependent electron density and the time-dependent one-body external potential for a given initial state. This correspondence is established through a universal but unknown action functional which depends on the density in a temporally nonlocal manner. The adiabatic approximation is often invoked, whereby the nonlocal time dependence of the action functional is neglected. With this approximation, the unknown action functional can be related directly to the exchange-correlation functional used in conventional Kohn-Sham density functional theory. The further approximation of linear response is also often invoked, neglecting higher-order contributions to the time-evolving density. Casida has shown how TDDFT within the linear response and adiabatic approximations may be efficiently implemented as a linear algebra problem,[2] and most applications of TDDFT in the context of quantum chemistry have used these approximations. Since the linear response states of TDDFT consist of single excitations from the Kohn-Sham reference determinant, the computational cost is comparable to Hartree-Fock based single excitation methods[7] such as configuration interaction with single excitations (CIS). Nevertheless, electron correlation is correctly treated in principle,[8] leading to a much-improved description of excitation energies compared to CIS methods.

It is important to recognize that there are a few significant problems with TDDFT in its current implementations. Vertical excitation energies to Rydberg states and long-range charge-transfer states are not accurately predicted.[9,10] Excited states with dominantly doubly excited character are poorly described, if at all.[11–14] The topology of the potential energy surface around intersections between the reference state and the lowest excited state is incorrectly described. In fact, when restricted closed-shell Kohn–Sham is used to describe the ground state, it can be shown that *conical* intersections of the ground and excited states do not exist in TDDFT using the linear response and adiabatic approximations.[13] This nonexistence of conical intersections traces back to an analog of Brillouin's theorem for TDDFT in the linear response and adiabatic approximations. For open shell molecules, where Brillouin's theorem does not strictly forbid conical intersections, the region of the potential energy surface around the intersections has been found to be grossly misshapen. In spite of these limitations, TDDFT gives useful results for vertical excitation energies to valence states which are singly excited relative to the ground state.[5] Furthermore, all of these problems are in principle due to inaccuracies of known approximations to the exchange-correlation functional. Thus, one can hope that they will be alleviated as more accurate exchange-correlation functionals are discovered.

While TDDFT is much less computationally demanding than alternative wavefunction-based *ab initio* methods of similar or better accuracy, such as multireference second-order perturbation theory[15] (e.g., CASPT2), it is nevertheless significantly more expensive than the preceding ground state DFT calculation. This poses a major obstacle to application of TDDFT in excited state calculations of large-scale sys-

a)Author to whom correspondence should be addressed. Phone: 217-333-1449. Electronic mail: tjm@spawn.scs.uiuc.edu.

tems. Hence, there is considerable impetus to find more efficient implementation schemes. In this paper, we apply the pseudospectral approximation for two-electron integral evaluation within the TDDFT framework. In the pseudospectral method,[16] two-electron integrals are factorized into intermediate quantities, using both spectral basis functions and physical space grid points. Since the Coulomb singularity is treated in the spectral basis, the required number of grid points for a given accuracy is significantly reduced compared to a purely numerical integration scheme. Because of this factorization, the formal scaling behavior of TDDFT is changed from $O(N^4)$ to $O(N^3)$, where N is a measure of the molecular size. The pseudospectral method has already been used extensively in both wavefunction- and density-based electronic structure methods.[16–25]

The performance of the new pseudospectral TDDFT (PS-TDDFT) method is explored for a variety of molecular systems including polyene oligomers, firefly luciferin, and microsolvated clusters of the chromophore of photoactive yellow protein (PYP). Considerable savings in computational cost is achieved with virtually no loss of accuracy in vertical excitation energies.

THEORY

Time-dependent density functional theory

We only briefly review the linear response TDDFT equations, since adequate treatments exist in the literature.[2] As in Kohn–Sham DFT (KS-DFT), TDDFT defines a reference system of noninteracting electrons whose one-electron density is identical to that of interacting electrons. Since the interacting and noninteracting systems share the same density, the same one-body external potential applies, and, thus, one can determine time evolution of a many-body wavefunction by solving an effective one-body time-dependent Schrödinger equation (the time-dependent Kohn–Sham equation):

$$i\frac{\partial}{\partial t}\varphi(r,t)=\left(-\frac{\nabla^2}{2}+\nu_{\mathrm{KS}}(r,t)\right)\varphi(r,t), \tag{1}$$

$$\nu_{\mathrm{KS}}[\rho,\Phi(0)](r,t)=\nu_{\mathrm{ext}}[\rho,\Psi(0)](r,t)+\int d^3r'\frac{\rho(r',t)}{|r-r'|}+\nu_{\mathrm{XC}}[\rho,\Psi(0),\Phi(0)](r,t). \tag{2}$$

In Eq. (2), the initial state dependence of exact time-dependent density functionals is explicitly shown: $\Psi(0)$ and $\Phi(0)$ are the initial state for the interacting system and the noninteracting KS system, respectively. The time-dependent external potential is given as $\nu_{\mathrm{ext}}(r,t)$. The second term in Eq. (2) corresponds to the classical Coulomb interaction, and the third term is the unknown time-dependent exchange-correlation functional. This functional establishes a mapping between the systems of interacting and noninteracting electrons that share the same electron density. The adiabatic approximation amounts to using the ground state exchange-correlation functional $E_{\mathrm{xc}}[\rho_t]$ for the time-dependent exchange-correlation potential, ignoring the initial state dependence of the density evolution.

$$\nu_{\mathrm{XC}}[\rho,\Psi(0),\Phi(0)](r,t)\approx\nu_{\mathrm{XC}}[\rho](r,t)\approx\frac{\delta E_{\mathrm{xc}}[\rho_t]}{\delta\rho_t(r)}. \tag{3}$$

Since $E_{\mathrm{xc}}[\rho_t]$ is locally time dependent, the exchange-correlation kernel f_{xc} in the adiabatic approximation is formulated accordingly, i.e.,

$$f_{\mathrm{xc}}[\rho](rt,r't')=\frac{\delta\nu_{\mathrm{xc}}[\rho](r,t)}{\delta\rho(r',t')}\delta(t-t'), \tag{4}$$

where δ in the first term denotes functional differentiation and in the second term it denotes the Dirac delta function. Within the time-dependent formalism above, excitation energies can be characterized as poles of the frequency-dependent response functions, e.g., dynamic polarizability. Casida has developed a method that converts the search for the poles into a large eigenvalue problem,[2] which closely resembles time-dependent Hartree–Fock approaches.[26] In this scheme, the TDDFT working equation is as follows.

$$\begin{pmatrix}\mathbf{A} & \mathbf{B}\\ \mathbf{B} & \mathbf{A}\end{pmatrix}\begin{pmatrix}\mathbf{X}\\ \mathbf{Y}\end{pmatrix}=\omega\begin{pmatrix}1 & 0\\ 0 & -1\end{pmatrix}\begin{pmatrix}\mathbf{X}\\ \mathbf{Y}\end{pmatrix}, \tag{5}$$

where

$$A_{ai\sigma,bj\tau}=\delta_{\sigma\tau}\delta_{ij}\delta_{ab}(\varepsilon_{a\sigma}-\varepsilon_{i\sigma})+K_{ai\sigma,bj\tau}-\delta_{\sigma\tau}c_{\mathrm{HF}}(a_\sigma b_\tau|j_\tau i_\sigma), \tag{6}$$

$$B_{ai\sigma,bj\tau}=K_{ai\sigma,jb\tau}-\delta_{\sigma\tau}c_{\mathrm{HF}}(a_\sigma j_\tau|b_\tau i_\sigma), \tag{7}$$

$$K_{kl\sigma,mn\tau}=\int dr,dr'\,\phi^*_{k\sigma}(r)\phi_{l\sigma}(r)\times\left(\frac{1}{|r-r'|}+(1-c_{\mathrm{HF}})\frac{\delta^2E_{\mathrm{XC}}}{\delta\rho_\sigma(r)\delta\rho_\tau(r')}\right)\times\phi^*_{n\tau}(r')\phi_{m\tau}(r'). \tag{8}$$

In Eqs. (6)–(8), σ and τ denote orbital spin and ω is the excitation energy. Mulliken notation has been used for the two-electron integrals.[27] The labels i,j and a,b represent occupied and virtual molecular orbitals in the KS determinant, and X_{ai} and Y_{ai} represent the components of the first-order response of density matrix associated with the orbital products $\phi_a\phi_i^*$ and $\phi_i\phi_a^*$, respectively. Finally, c_{HF} is the coefficient for exact Hartree–Fock exchange in hybrid functionals. Hirata and Head–Gordon showed that the Tamm–Dancoff approximation (TDA), which amounts to neglecting $\mathbf{Y}$ in Eq. (5), can often accurately reproduce the results of TDDFT.[28] The TDA/TDDFT working equation becomes

$$\mathbf{AX}=\omega\mathbf{X}, \tag{9}$$

from which the CIS equation can be obtained if c_{HF} in Eqs. (6) and (8) is equal to unity. For TDA/TDDFT with hybrid functionals, the exchange integrals scaled by the coefficient c_{HF} must be evaluated in addition to integrals involving the exchange-correlation functional. The structure of the equations makes it clear that the computational complexity of TDA/TDDFT is similar to that of CIS.

Pseudospectral evaluation of two-electron integrals

The $O(N^4)$ scaling of two-electron integral evaluation is a significant computational bottleneck for the applications of TDDFT to large-scale systems. To solve similar scaling problems, the pseudospectral approach has been used in wide variety of correlated wavefunction-based methods as well as in KS-DFT. A general review of the pseudospectral method has been presented elsewhere.[16] Here, we discuss some essential points of the method for completeness.

The pseudospectral method provides an alternative way of dealing with the two-electron integrals. Consider the general form of two-electron repulsion integrals in terms of spectral basis functions φ_i,

$$(ab|cd) = \int \frac{\varphi_a(\mathbf{r}_1)\varphi_b(\mathbf{r}_1)\varphi_c(\mathbf{r}_2)\varphi_d(\mathbf{r}_2)}{|\mathbf{r}_1 - \mathbf{r}_2|} d\mathbf{r}_1 d\mathbf{r}_2. \tag{10}$$

In electronic structure methods, these integrals are always used in contracted form. For example, in the notation of Eqs. (5)–(8), one term which needs to be computed in TDDFT is

$$(\mathbf{AX})_{ai} + = \sum_{bj} (ai|bj)\mathbf{X}_{bj}, \tag{11}$$

scaling as $O(N^4)$, where N is the number of orbitals and we make no distinctions (for the purpose of the scaling analysis) between occupied and virtual orbitals. If the integrals can be factorized as

$$(ab|cd) = \sum_{g=1}^{N_s} Q_{ag} A_{cdg} R_{gb}, \tag{12}$$

then Eq. (11) can instead be evaluated as

$$(\mathbf{AX})_{ai} + = \sum_{g} Q_{ag} R_{gi} \sum_{bj} A_{bjg} \mathbf{X}_{bj}, \tag{13}$$

which scales as $O(N_g N^2)$, where N_g is the number of intermediate terms in the factorization. Provided the number of intermediate terms N_g is of the same order as the number of orbitals N, this represents a scaling advantage of N. Of course, there are a number of different ways to obtain a factorization similar to the form shown in Eq. (12). For example, pseudospectral methods,[16] Cholesky factorization,[29] and resolution-of-the-identity[30–34] (RI) approaches are all based on this idea. As discussed below, the factorization resulting from Cholesky and RI approaches is more restrictive than Eq. (12). This restriction limits the gains which can be obtained using Cholesky and RI approaches,[20] but recent work has addressed this problem in the case where localized orbitals are used.[35]

The pseudospectral method is closely related to numerical integration, but with a different perspective rooted in the idea of forward and backward transformations between spectral space (coefficients of basis functions) and physical space (function values on a grid) representations. This perspective allows higher accuracy for a given number of grid points and is a key to the success of the pseudospectral method in electronic structure theory. The quantities used in the integral factorization are

$$R_{ga} = \varphi_a(\mathbf{r}_g), \tag{14}$$

$$A_{cdg} = \int \frac{\varphi_c(\mathbf{r})\varphi_d(\mathbf{r})}{|\mathbf{r} - \mathbf{r}_g|} d\mathbf{r}, \tag{15}$$

$$\mathbf{Q} = \mathbf{S}(\mathbf{R}^t\mathbf{w}\mathbf{R})^{-1}\mathbf{R}^t\mathbf{w}, \tag{16}$$

where $\mathbf{r}_g$ denotes the position of a grid point, $\mathbf{S}$ is the overlap matrix of the basis functions, and $\mathbf{w}$ is a diagonal matrix of grid weights. If the physical to spectral transformation matrix $\mathbf{Q}$ is replaced by

$$\mathbf{Q} = \mathbf{R}^t\mathbf{w}. \tag{17}$$

The resulting integral factorization is equivalent to evaluating the two-electron integrals by numerical integration over the coordinates of one of the electrons and analytic integration over the coordinates of the other electron.

Since both spectral and physical spaces are incomplete, transformation between them can cause errors, which are analogous to so-called aliasing in discrete Fourier transform theory.[36] Aliasing errors can be effectively removed by correcting the incompleteness of either space using dealiasing functions which are orthogonal to the basis set. Including the dealiasing functions in $\mathbf{R}$ and $\mathbf{S}$, one can analytically project out the aliasing terms in the inverse transformation from physical space to spectral space.

As noted above, integral factorization can also be achieved by Cholesky or RI methods. In this case, the factorization is more restrictive,

$$(ab|cd) = \sum_{\kappa}^{N_\kappa} B_{ab\kappa} A_{cd\kappa}, \tag{18}$$

where

$$B_{abk} = \int \varphi_a(\mathbf{r})\varphi_b(\mathbf{r})\kappa(\mathbf{r}) d\mathbf{r},$$

$$A_{cdk} = \int \frac{\kappa(\mathbf{r}_1)\varphi_c(\mathbf{r}_2)\varphi_d(\mathbf{r}_2)}{|\mathbf{r}_1 - \mathbf{r}_2|} d\mathbf{r}_1 d\mathbf{r}_2, \tag{19}$$

and $\kappa(\mathbf{r})$ are the auxiliary basis functions. We have specified to the RI case in the preceding, but the basic structure is the same in a Cholesky decomposition approach. Because the factorization of Eq. (18) does not separate the indices as much as that of Eq. (12), there is no scaling advantage in dealing with exchange terms. Recently, Furche has introduced an implementation of TDDFT within the RI approximation,[37] which accomplishes a factorization similar to the pseudospectral one for the Coulomb terms, but is not able to provide similar savings when hybrid[38] and/or long-range corrected[39] functionals are used, because then exchange terms are present which resist factorization within the RI method.

For completeness, we also mention the Sternheimer approach to TDDFT which has recently been proposed[40,41] as an alternative formulation of TDDFT based on density functional perturbation theory.[42] The Sternheimer approach is not an integral factorization approximation like the methods discussed above. Its relevance in the present context comes about because it scales quadratically with system size when implemented in real space.[41] The method does not provide

excitation energies directly, but rather the dynamic polarizability. Determining the excitation energies from the dynamic polarizability necessitates scanning over the frequency range to locate the poles. Furthermore, the method converges very slowly for frequencies in the vicinity of poles. Thus, the Sternheimer method is not well suited to precise computation of few low-lying excited states, as often desired in the chemical context. However, it is an attractive alternative to the pseudospectral method we discuss here when the dynamic polarizability over a large frequency range is desired.

PS-CIS and PS-TDA/TDDFT have been implemented in JAGUAR with a direct configuration interaction (CI) scheme,[43] and direct evaluation of the required integrals in every iteration. In both CIS and TDA/TDDFT, the fundamental operation is the **AX** matrix-vector product, as shown in Eq. (9). The **A** matrix should be symmetric, but this is not necessarily so when the pseudospectral approximation is employed. A similar issue exists for the Fock matrix in pseudospectral self-consistent field methods. In the JAGUAR package, the Fock matrix of PS-KS-DFT is symmetrized[44] by utilizing the length scale of the basis functions involved to pick the more accurate of the matrix elements F_{ab} and F_{ba}. In PS-CIS and PS-TDDFT, we form the **AX** matrix-vector products without symmetrizing **A**, but instead symmetrizing the subspace Hamiltonian matrix generated by the iterative procedure.[45] This symmetrization can be done by averaging off-diagonal matrix elements or by using only the upper or lower triangles of the matrix (making the other block the same). We have investigated these different ways of symmetrizing for a number of test molecules using coarse grids, *vide infra*, and the mean absolute deviation (MAD) of vertical excitation energies is only 0.0046 eV. For comparison, the MAD from the spectral calculations is 0.0142 and 0.0157 eV for averaging and nonaveraging PS calculations, respectively. Using denser grids, the MAD of the averaging and nonaveraging symmetrizations is 0.0009 eV, while the MAD of the spectral and pseudospectral results becomes 0.0102 eV for both cases. We conclude that the details of symmetrization are not critical and we use only the lower triangle of the subspace Hamiltonian in the data presented below.

Our implementation of PS-CIS and PS-TDA/TDFT applies the pseudospectral approximation to the CIS and TDA/TDDFT equations previously detailed in the literature.[7,28] The fundamental matrix-vector product in CIS in the molecular orbital (MO) basis (ignoring spin for simplicity) is

$$(\mathbf{A}^{\mathrm{CIS}}\mathbf{X})_{bj} = \sum_{ai} [\delta_{ab}\delta_{ij}(\varepsilon_a - \varepsilon_i) + (ai|jb) - (ab|ji)]X_{ai}. \tag{20}$$

The last two terms involving two-electron integrals in the MO basis can be written in the atomic orbital (AO) basis as follows:[7]

$$\sum_{ia} \{(ai|jb) - (ab|ji)\}X_{ia} = \sum_{\mu\nu} C_{\mu j}C_{\nu b}F_{\mu\nu}, \tag{21}$$

$$F_{\mu\nu} = \sum_{\lambda\theta} T^{\mathrm{CIS}}_{\lambda\theta}\{(\mu\lambda|\nu\theta) - (\mu\nu|\lambda\theta)\},$$
$$T^{\mathrm{CIS}}_{\lambda\theta} = \sum_{ia} X_{ia}C_{\lambda i}C_{\theta a}. \tag{22}$$

In Eqs. (21) and (22), μ, ν, λ, and θ refer to AOs and $C_{\lambda i}$ denotes the MO coefficients. $\mathbf{T}^{\mathrm{CIS}}$ is a transition density matrix (which is not symmetric) from the ground state to the excited states. Since the MO coefficients are already obtained in the preceding self-consistent field (SCF) calculation, most of the computational cost of the **AX** matrix-vector multiplication resides in the evaluation of Fock matrix elements $F_{\mu\nu}$, in which the required AO integrals are recalculated every iteration. In the PS-CIS approach, the Fock matrix elements are formulated as follows:

$$\sum_{\lambda\theta} T^{\mathrm{CIS}}_{\lambda\theta}(\mu\lambda|\nu\theta) = \sum_{\lambda\theta g} T^{\mathrm{CIS}}_{\lambda\theta}Q_{\mu g}R_{g\lambda}A_{\nu\theta g} = \sum_{g} Q_{\mu g}\left[\sum_{\theta} A_{\nu\theta g}\left(\sum_{\lambda} R_{g\lambda}T^{\mathrm{CIS}}_{\lambda\theta}\right)\right], \tag{23}$$

$$\sum_{\lambda\theta} T^{\mathrm{CIS}}_{\lambda\theta}(\mu\nu|\lambda\theta) = \sum_{\lambda\theta g} T^{\mathrm{CIS}}_{\lambda\theta}Q_{\mu g}R_{g\nu}A_{\lambda\theta g} = \sum_{g} Q_{\mu g}R_{g\nu}\left(\sum_{\lambda\theta} A_{\lambda\theta g}T^{\mathrm{CIS}}_{\lambda\theta}\right). \tag{24}$$

This uses much of the same code for ground state Fock matrix construction in JAGUAR, with the added complication that the density matrix is not symmetric. Both terms scale as $O(MN^2)$ with M grid points. Since M is usually on the order of N, an order of reduction in formal scaling is achieved in the PS-CIS and, thus, PS-TDA/TDDFT. The exchange-correlation term of PS-TDA/TDDFT is treated with a pure numerical integration, analogous to conventional DFT and TDDFT methods.

The JAGUAR program contains two kinds of physical space grids—pseudospectral grids[46,47] which are meant for use with corresponding dealiasing sets within the pseudospectral approximation, and DFT grids[22] which are meant for use in numerical integration of the exchange-correlation functional. In both cases, the grids are atom centered and the final molecular grid is the union of the atomic grids subject to a pruning step. The details of grid optimization, construction, and pruning can be found elsewhere. We simply state that the angular grid densities for each radial shell in an atom follow the Stroud–McLaren[48] or Lebedev[49] constructions that integrate a specified maximum degree of spherical harmonics exactly. Placement of the radial shells follows one of several possible schemes[50–53] and the interested reader is referred to the literature and/or the JAGUAR manual for details. For both the pseudospectral and DFT grids, at least three different resolutions are available—referred to as coarse, medium, and fine in the following. The grid weights **w** in the pseudospectral method are set to be the angular weights multiplied by the volume of radial shells, and Voronoi polyhedra are used to construct molecular grids.[46] In the DFT grids, **w** is scaled by Becke's normalized cell functions, and molecular integrals are calculated accordingly.[54] In contrast to the

pseudospectral grids, DFT grids are not basis set/atom dependent for the first and second row atoms except that they are more extended when diffuse basis functions are used. In the following, the pseudospectral and DFT grids are referred to with bold letters and distinguished by capitalization, with lower case for the PS grids and upper case for the DFT grids. Thus, the pseudospectral coarse grid is denoted **c** and the DFT coarse grid is denoted **C**.

Note that it is possible to use the PS grids in a pure numerical integration scheme, i.e., the use of DFT or PS grids does not necessarily imply the use of pure integration or pseudospectral approximations in the resulting equations. In fact, we will use both PS and DFT grids in the numerical integration of the exchange-correlation contribution to PS-TDA/TDDFT in the following results. The Coulomb and exchange terms arising in Eqs. (23) and (24) are always treated using the pseudospectral approximation (necessitating the use of PS grids since these have associated dealiasing sets).

RESULTS

The PS-TDA/TDDFT (PS-TDDFT, hereafter) method has been implemented in a development version of JAGUAR program package,[55] which we have used for all test results shown here. However, the method is now also available in the latest release of JAGUAR 7.0. A set of conjugated polyenes, firefly luciferin, and aqueous microsolvated clusters of the chromophore of PYP were chosen as test systems. Luciferin is a biological pigment in luminescent organisms that emit light from catalytic oxidation using luciferase and adenosine triphosphate (ATP).[56] PYP is a bacterial light receptor protein, which is responsible for the negative phototactic behavior of *Halorhodospira halophila* in the presence of blue light.[57] Figure 1 shows the structure of these molecules. For each of the test molecules, ground state optimized geometries were obtained using KS-DFT with the B3LYP (Ref. 38) functional. An exception is the microsolvated PYP chromophore, where geometries were obtained using semiempirical quantum mechanical/molecular mechanical (QM/MM) Brownian dynamics equilibration at 300 K for 1 ps. In these QM/MM calculations, the chromophore constitutes the QM region and is treated with the PM3 Hamiltonian,[58] while the remaining water molecules are represented using the SPC force field.[59] These QM/MM calculations were carried out with a development version of the MOPAC package.[60] The full pseudospectral capabilities of JAGUAR were used in the KS-DFT part of the PS-TDDFT calculation, including Fock matrix updating[61] with a multigrid strategy,[44] analytic two-electron integral corrections, and the length scale algorithm.[50] None of these advanced techniques was used in the PS-TDDFT calculations. It is expected that the results shown here can be made more accurate and/or efficient by implementation of some of these advanced techniques in the future.

The PS-TDDFT calculations use the pseudospectral approximation for the Coulomb and exchange terms of the Fock matrix, Eqs. (23) and (24), in each iteration. Evaluation of the exchange-correlation functional contribution to the **A** matrix, Eqs. (6) and (8), is accomplished in a *pure* numerical

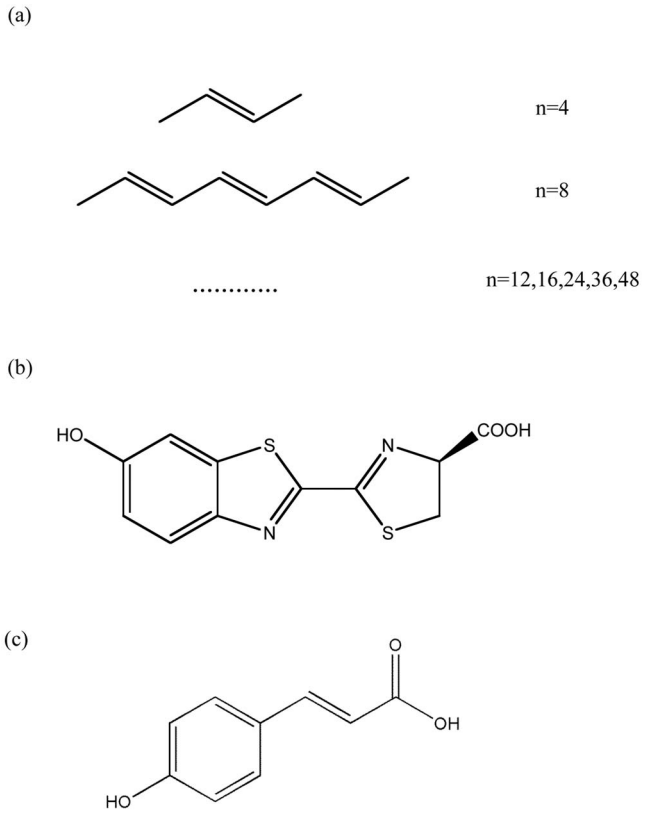

FIG. 1. Schematic structures of (a) the conjugated polyenes (C_nH_{n+2}), (b) firefly luciferin ($C_{11}H_8O_3N_2S_2$), and (c) the chromophore of photoactive yellow protein ($C_9H_8O_3$).

integration scheme with $\mathbf{Q}=\mathbf{R}^t\mathbf{w}$. Following the notation introduced above, we have used four different grids in the PS-TDDFT calculations—pseudospectral coarse and medium (**c** and **m**, respectively) and DFT coarse and medium (**C** and **M**, respectively).[62] As discussed above, the **c** and **m** grids were originally designed for pseudospectral evaluation of the Coulomb and exchange contributions, while the **C** and **M** grids were designed for the numerical integration of K_{xc} in KS-DFT. The two grids used in a PS-TDDFT calculation are designated in parenthesis. For example, (**c**,**C**) denotes the use of the pseudospectral coarse grid for Coulomb and exchange evaluation and the DFT coarse grid for numerical integration of the exchange-correlation contribution.

Tables I and II list the size of the grids and basis sets used for the test molecules. This table shows that the **c**, **m**, **C**, and **M** grids contain approximately 50, 250, 500, and 1500 points per atom, respectively. The 6-31++G** basis set is used for the conjugated polyenes. For luciferin, we use two different basis sets indicated in Table I, and for the microsolvated PYP chromophore, the 6-31G* basis set is used. The results of TDA-TDDFT vertical excitation energy calculations using the B3LYP functional for the conjugated polyenes and luciferin are shown in Table III. The vertical excitation energies are compared for our own spectral code (implemented within JAGUAR) and Q-CHEM 3.0,[63] showing the correctness of our spectral implementation. The small differences between the two spectral codes are a result of differing integral evaluation and convergence thresholds, with the maximum discrepancy being 0.04 eV. We also show

TABLE I. Size of the grids and basis sets used in TDDFT calculations on conjugated polyenes (with n carbon atoms) and firefly luciferin.

	Total number of grid points				
n	**c**	**m**	**C**	**M**	No. of basis functions
4	740	3216	7628	21280	112
8	1374	6030	13692	38304	212
12	2006	8850	19756	55328	312
16	2626	11668	25820	72352	412
24	3870	17306	37948	106400	612
36	5742	25756	56140	157472	912
48	7614	34169	74332	208544	1212
Luciferin					
6-311G**	2252	5482	18326	30992	388
6-311++G**	2214	11933	19642	55900	398

results from PS-TDDFT calculations using different combinations of grids. For luciferin, we were not able to use the **c** grid in pseudospectral evaluation of the Coulomb/exchange contribution because of convergence difficulties. This is likely due to insufficient optimization of dealiasing sets for the sulfur atom, but should be investigated further in the future.

The error incurred by the pseudospectral approximation using the smallest possible grids never exceeds 0.04 eV. Indeed, the mean absolute deviation (MAD) of the spectral and pseudospectral results is only 0.0137 eV for (**c**,**c**) grid and 0.0035 eV for (**m**,**c**) grid. Both of these deviations are well within the accuracy of the TDA-TDDFT method itself given present functionals and certainly within chemical accuracy for excitation energies. As expected, the MADs decrease when larger grids are used, falling to 0.013, 0.013, 0.002, and 0.002 eV for the (**c**,**C**), (**c**,**M**), (**m**,**C**), and (**m**,**M**) grids, respectively. Generally, the smallest possible grids are the (**c**,**c**) class, which implies usage of the pseudospectral coarse grid for pure numerical integration of the exchange-correlation contribution. Although the **M** grid has more than 20 times as many points as the coarsest grid **c**, the difference in the excitation energies is chemically insignificant when those grids are used for the evaluation of the exchange-correlation functional contribution. Such small grids are certainly inadequate in ground state DFT, suggesting that the grid requirements for integration of the exchange-correlation functional are not the same in DFT and TDDFT. This is in contrast to the conventional wisdom and we therefore suggest that it might be fruitful to investigate the use of sparse grids for the exchange-correlation contribution to TDDFT even in conventional spectral algorithms. This is in accord with previous experience in applying pseudospectral approximations to correlated wavefunction-based methods.[17–21] The correlation correction is much smaller in absolute value than the SCF energy. The chemical accuracy criterion is generally expressed as an absolute energy, e.g., 1 kcal/mol. Thus, one requires less relative accuracy when determining the correlation correction compared to that required when determining the SCF energy. For numerical integration schemes, this means one can use sparser grids for the correlation correction than for the SCF contribution.

TABLE II. Size of the grids and basis sets used in TDDFT calculations on the isolated and microsolvated chromophore of the photoactive yellow protein (PYP).

	Total number of		
No. of H_2O	grid points (**c**)	basis functions	atoms
0	1693	196	20
10	4045	386	50
20	6337	576	80
30	8728	766	110
40	10941	956	140
50	13148	1146	170

The computational effort in CIS and TDDFT is dominated by the **AX** matrix-vector multiplication step. To assess the computational efficiency of PS-TDDFT, Table IV compares CPU times for this step for the polyenes and luciferin. These calculations were all carried out on an AMD Opteron 175 CPU. It is clear that our own spectral algorithm is not particularly efficient as compared to Q-CHEM. This is not surprising, since we have not yet expended much effort to optimize either the spectral or pseudospectral implementations. For example, we calculate all terms in the **AX** product with no attempt to use thresholds to ignore terms that are numerically insignificant. Such optimizations will be pursued in the future. Nevertheless, the PS-TDDFT method can be more than four times faster than Q-CHEM, and more than ten times faster than our own spectral implementation. The gains in the pseudospectral approach increase as molecular size increases, as expected when a scaling advantage is present.

The savings from the pseudospectral approach is not limited to hybrid functionals. In Table V, we compare CPU times for the polyenes using CIS, SVWN,[64,65] and BLYP,[66,67] functionals. The pseudospectral method is seen to be even more advantageous for the less complicated functionals. However, this is likely a consequence of the fact that we have not optimized the code for the numerical integration of the exchange-correlation contribution.

Figure 2 compares the CPU time per iteration for the B3LYP/TDDFT calculations of the polyenes using our spectral implementation and the pseudospectral implementation with various grid sizes. There is still room for speeding up the iterative diagonalization, for example, by updating the CIS Fock matrix with a multigrid scheme, i.e., using a combination of sparse and dense grids during the iterative procedure. Note that the **c** grid was optimized for atomic pseudospectral calculation of **J** and **K** integrals with a given spectral basis set and dealiasing functions. Further reduction of the number of grid points can be expected by TDDFT-specific optimization of the grids for K_{xc} integrals. This is also the case in a spectral TDDFT calculation. For example, replacing the default grid **C** for K_{xc} integrals of the spectral TDDFT calculations with the PS coarse grid **c** gives a MAD of 0.0075 eV from spectral calculations for the lowest three excited states in a set of molecules shown in Table VI. Grid **C** has nine to ten times more grid points than grid **c**, and the spectral TDDFT with grid **c** is about two times faster than with grid **C**. From Tables III–V, it can be seen that the two

TABLE III. TDA-TDDFT vertical excitation energies using the B3LYP functional of conjugated polyenes (with n carbon atoms) and firefly luciferin.

		TDA-TDDFT Excitation Energy/eV					
polyenes		Pseudospectral			Spectral		Absolute deviation
n		(**c**,**c**)	(**c**,**C**)	(**c**,**M**)	**C**	Q-CHEM	|Spectral-(**c**,**c**)|
4	S_1	5.7279	5.7131	5.7131	5.7079	5.6706	0.0200
	S_2	5.9393	5.9340	5.9319	5.9584	5.9480	0.0191
	S_3	5.9754	5.9684	5.9685	5.9936	5.9861	0.0182
	S_4	6.0645	6.0524	6.0510	6.0507	6.0310	0.0138
8	S_1	4.3476	4.3485	4.3475	4.3864	4.3819	0.0388
	S_2	4.8134	4.8123	4.8125	4.8129	4.8147	0.0005
	S_3	4.9283	4.9255	4.9261	4.9166	4.9117	0.0117
	S_4	4.9863	4.9751	4.9757	4.9696	4.9204	0.0167
12	S_1	3.4825	3.4830	3.4824	3.5123	3.5073	0.0298
	S_2	3.7373	3.7365	3.7368	3.7333	3.7344	0.0040
	S_3	4.5058	4.5039	4.5047	4.4975	4.4909	0.0083
	S_4	4.6631	4.6544	4.6554	4.6504	4.5977	0.0127
16	S_1	2.9337	2.9340	2.9335	2.9580	2.9509	0.0243
	S_2	3.0942	3.0936	3.0938	3.0894	3.0908	0.0048
	S_3	4.0727	4.0718	4.0720	4.0574	4.0592	0.0153
	S_4	4.4080	4.4074	4.4083	4.4247	4.4264	0.0167
24	S_1	2.2773	2.2774	2.2771	2.2965	2.2840	0.0192
	S_2	2.3813	2.3808	2.3809	2.3756	2.3799	0.0057
	S_3	3.0986	3.0980	3.0981	3.0887	3.0912	0.0099
	S_4	3.2964	3.2962	3.2960	3.3107	3.3144	0.0143
36	S_1	1.7692	1.7692	1.7690	1.7798	1.7728	0.0106
	S_2	1.8798	1.8794	1.8795	1.8762	1.8796	0.0036
	S_3	2.3710	2.3706	2.3707	2.3662	2.3687	0.0048
	S_4	2.4884	2.4887	2.4885	2.4963	2.4993	0.0079
48	S_1	1.5039	1.5040	1.5038	1.5270	1.5046	0.0231
	S_2	1.6277	1.6274	1.6275	1.6132	1.6298	0.0145
	S_3	1.9919	1.9917	1.9917	1.9796	1.9924	0.0123
	S_4	2.0668	2.0670	2.0669	2.0649	2.0767	0.0019
Luciferin		(**m**,**c**)	(**m**,**C**)	(**m**,**M**)			|Spectral-(**m**,**c**)|
6-311G**	S_1	3.8891	3.8890	3.8887	3.8918	3.8904	0.002
	S_2	4.0662	4.0640	4.0641	4.0697	4.0680	0.0035
	S_3	4.1584	4.1576	4.1576	4.1583	4.1571	0.0001
	S_4	4.4808	4.4915	4.4913	4.4900	4.4876	0.0092
6-31++G**	S_1	3.8868	3.8871	3.8869	3.8877	3.8848	0.0009
	S_2	4.0586	4.0566	4.0567	4.0601	4.0557	0.0015
	S_3	4.1424	4.1423	4.1423	4.1430	4.1397	0.0006
	S_4	4.4913	4.5023	4.5021	4.5005	4.4999	0.0092

coarsest combinations of grid (**c**,**c**) and (**m**,**c**) give an efficient and accurate way of calculating the TDDFT excitation energies for molecules containing first and second row atoms.

The polyenes are quasi-one-dimensional molecules, and, thus, one might expect somewhat special behavior as concerns the scaling of the algorithms (although we have not used symmetry explicitly in any of the calculations in this paper). Thus, we have also chosen a series of test molecules which are fully three dimensional—microsolvated water clusters of the PYP chromophore [see Fig. 1(c)]. Table VII shows both excitation energies and CPU timings for these microsolvated clusters. Our tests include the PYP chromophore in isolation and surrounded by up to 50 water molecules (which is almost two complete solvation shells). The size of the grids used and the number of basis functions for each cluster are given in Table II. For the polyenes and firefly luciferin, we calculated the lowest four singlet valence-excited states to see how accurately the method predicts the excitation energies with different grid combinations. Here, we focus on the lowest optically active, i.e., bright, state which would dominate the absorption spectrum. It is of interest to determine if solvation shifts can also be well predicted (as are the absolute vertical excitation energies them-

TABLE IV. Comparison of CPU times for **AX** matrix-vector multiplication in TDA-TDDFT calculations of Table III using pseudospectral and spectral methods. The (**c**,**c**) grids and B3LYP functional are used. Timings for the conventional spectral algorithm are shown using Q-CHEM and our own implementation ("spectral").

	AX CPU Time (s)				
	Pseudospectral			Spectral	
Polyenes	(**c**,**c**)	(**c**,**C**)	(**c**,**M**)	**C**	Q-CHEM
$n=4$	2	12	29	18	3
$n=8$	10	44	108	99	15
$n=12$	25	87	207	274	40
$n=16$	43	135	319	551	78
$n=24$	84	247	571	1397	191
$n=36$	174	466	1082	3445	457
$n=48$	280	751	1750	6488	1671
Luciferin	(**m**,**c**)	(**m**,**C**)	(**m**,**M**)		
6-31++G**	80	188	407	682	103
6-311G**	48	102	135	423	70

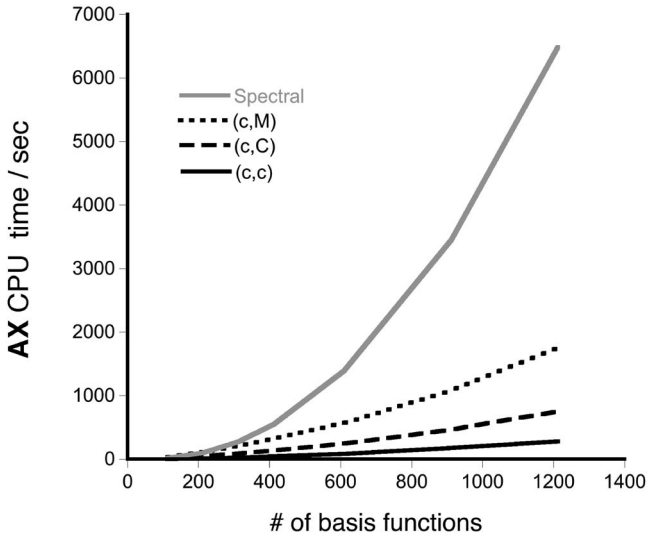

FIG. 2. CPU times per iteration for TDA/TDDFT(B3LYP)/6-31++G** calculations on polyene oligomers presented in Table IV. Spectral (gray line) and pseudospectral (black lines) TDDFT with different numerical integration grids for evaluating the integrals with the exchange-correlation kernel are shown. See Table I for the size of the grids.

selves) within the pseudospectral approximation. We have used the CIS and TDA-TDDFT methods with the SVWN and B3LYP functionals for these test cases: As can be seen in Table VII, the agreement of both excitation energies and oscillator strengths is excellent. Furthermore, the excitation energy shift going from the isolated chromophore to a microsolvated cluster mimicking bulk solvation is also in excellent agreement. For example, the vertical excitation energy shift predicted by B3LYP-TDDFT going from the isolated chromophore to a cluster environment of 50 water molecules is 0.393 eV, when the psuedospectral approximation is used, and 0.396 eV for the purely spectral calculation. All of the reported calculations agree on a redshift of 0.3–0.4 eV upon solvation of the PYP chromophore, even though the absolute excitation energies are not in good agreement when using different functionals. The MADs from spectral results are 0.0058 eV and 0.0092 for excitation energies and oscillator strength, respectively. CPU times per iteration for these test cases involving the PYP chromophore are shown in Fig. 3(b), highlighting the savings from the pseudospectral method.

Another point of interest regarding the results in Table VII is the presence of many dark states below the optically bright state when the local density functional (SVWN) is used. These states correspond to long-range charge transfer from the chromophore to water molecules. Note that these spuriously low-lying excited states do not appear in CIS. B3LYP still suffers from this problem, but not as significantly as in SVWN for the testing cases. As discussed by Dreuw *et al.*,[10] this is expected because exact exchange is needed to obtain the correct Coulombic interaction between the transferred charges in TDDFT. It is perhaps surprising that B3LYP does not do worse here (since only a fraction of exact exchange is included). Because of the spurious charge-transfer states, we have omitted calculation results in Table VII for some of the clusters—if the bright state is found above the seventh excited singlet state, we did not calculate the result with the spectral method (other than to ensure that the bright state predicted by the spectral method was not among the first seven excited states). In the case with 50 water molecules surrounding the PYP chromophore, we did not continue the pseudospectral calculations after determining that the bright state did not lie within the first 30 excited states. Calculations which were not completed for these reasons are designated with "n/c" in Table VII. Recently, Tawada *et al.* proposed a long-range corrected

TABLE V. CPU time comparisons for CIS and TDDFT calculations with various exchange-correlation functionals for conjugated polyenes (with n carbon atoms) using the 6-31++G** basis set. PS-CIS and PS-TDDFT calculations use the **c** and (**c**,**c**) grids, respectively.

	AX CPU time (s)								
	CIS			SVWN			BLYP		
n	**c**	Q-CHEM	Spectral	(**c**,**c**)	Q-CHEM	Spectral	(**c**,**c**)	Q-CHEM	Spectral
4	1	1	7	1	2	6	2	3	16
8	2	9	57	2	12	42	10	15	81
12	5	29	191	5	35	135	23	40	213
16	10	61	423	9	68	293	41	78	404
24	23	162	1168	21	176	783	76	190	971
36	58	408	3055	51	429	1996	137	453	2300

TABLE VI. BLYP and B3LYP spectral TDA/TDDFT vertical excitation energies (eV) to the lowest three singlet valence states in four test molecules. Two different grids (**C** and **c**) are used for integration of the exchange-correlation functional, as discussed in the text. Ground state geometries in each case were optimized with B3LYP/KS-DFT using the same basis set as in the subsequent TDDFT calculations. The mean absolute deviation (MAD) of the spectral calculations with grid **c** from the spectral ones with grid **C** is 0.0075 eV, showing that the very sparse **c** grid provides sufficient accuracy.

	PYP 6-31G*		H_2O 6-31++G**		Butadiene 6-31++G**		Octatetraene 6-31++G**	
	C	**c**	**C**	**c**	**C**	**c**	**C**	**c**
				BLYP				
S_1	3.7309	3.7118	6.2478	6.2571	5.3328	5.3488	4.1449	4.1463
S_2	4.1740	4.1733	7.6060	7.6002	5.5737	5.5858	4.2421	4.2430
S_3	4.2432	4.2448	8.1393	8.1506	5.6224	5.6358	4.5537	4.5584
				B3LYP				
S_1	4.4728	4.4626	6.9004	6.9089	5.7079	5.7232	4.3864	4.3884
S_2	4.5194	4.5191	8.3792	8.3725	5.9584	5.9668	4.8129	4.8161
S_3	4.6934	4.6958	8.8330	8.8441	5.9936	6.0017	4.9166	4.9233

TDDFT(LC-TDDFT),[39] which aims at alleviating this problem by allowing long-range exchange interaction between distant orbitals. Implementation of LC-TDDFT within the framework of the pseudospectral method is currently in progress. Also, Zhao and Truhlar have introduced[68] a new functional (M06-HF) which includes full-strength exact exchange that has shown promising results in modeling charge-transfer and Rydberg excitations. This functional has already been implemented in the latest version of JAGUAR (7.0) and, thus, can be used with PS-TDDFT. Unfortunately, the improved performance for charge-transfer states comes at the expense of valence state excitation energies in the current parameterization.

TABLE VII. Vertical excitation energies of the chromophore of photoactive yellow protein in isolation and microsolvated environments with varying numbers of water molecules. The (**c**,**c**) grid was used for PS-TDDFT (B3LYP and SVWN). Spectral TDDFT calculations used the **C** grid for integration of the exchange-correlation functional. Calculations which were not completed because of excessive low-lying spurious charge-transfer states in TDDFT are denoted "n/c." See text for details.

B3LYP/6-31G*	**A**X CPU time (s)		Excitation energy to the lowest bright state					
			(**c**,**c**)			Spectral		
No. of H_2O	(**c**,**c**)	Spectral	Excitation energy (eV)		Oscillator strength	Excitation energy (eV)		Oscillator strength
0	10	66	S_2	4.5089	0.8890	S_2	4.5194	0.8949
10	34	410	S_1	4.1942	0.7124	S_1	4.2020	0.7205
20	96	660	S_2	4.2281	0.5841	S_2	4.2329	0.5979
30	173	1224	S_1	4.3553	0.5678	S_1	4.3580	0.5746
40	297	2226	S_1	4.1302	0.7609	S_1	4.1294	0.7635
50	482	3830	S_4	4.1156	0.8557	S_4	4.1236	0.8626
CIS/6-31G*	**A**X CPU time (s)		Excitation energy to the lowest bright state					
			c			Spectral		
0	2	37	S_1	5.1888	0.8030	S_1	5.1792	0.8166
10	9	138	S_1	4.9727	0.6638	S_1	4.9649	0.6713
20	25	434	S_1	5.2566	0.6813	S_1	5.2525	0.6978
30	52	809	S_1	5.1991	0.5657	S_1	5.1990	0.5780
40	100	1473	S_1	4.9701	0.7931	S_1	4.9612	0.8002
50	186	2938	S_1	4.7762	0.8138	S_1	4.7781	0.8271
SVWN/6-31G*	**A**X CPU time (s)		Excitation energy to the lowest bright state					
			(**c**,**c**)			Spectral		
0	2	30	S_1	4.1574	0.7171	S_1	4.1713	0.7252
10	9	113	S_7	3.8921	0.5785	S_7	3.8297	0.5756
20	27	349	S_{16}	3.7480	0.2786	n/c	n/c	n/c
30	52	680	S_1	3.8449	0.2204	S_1	3.8492	0.2057
40	93	1253	S_{14}	3.7517	0.6177	n/c	n/c	n/c
50	159	2425	$>S_{30}$	n/c	n/c	n/c	n/c	n/c

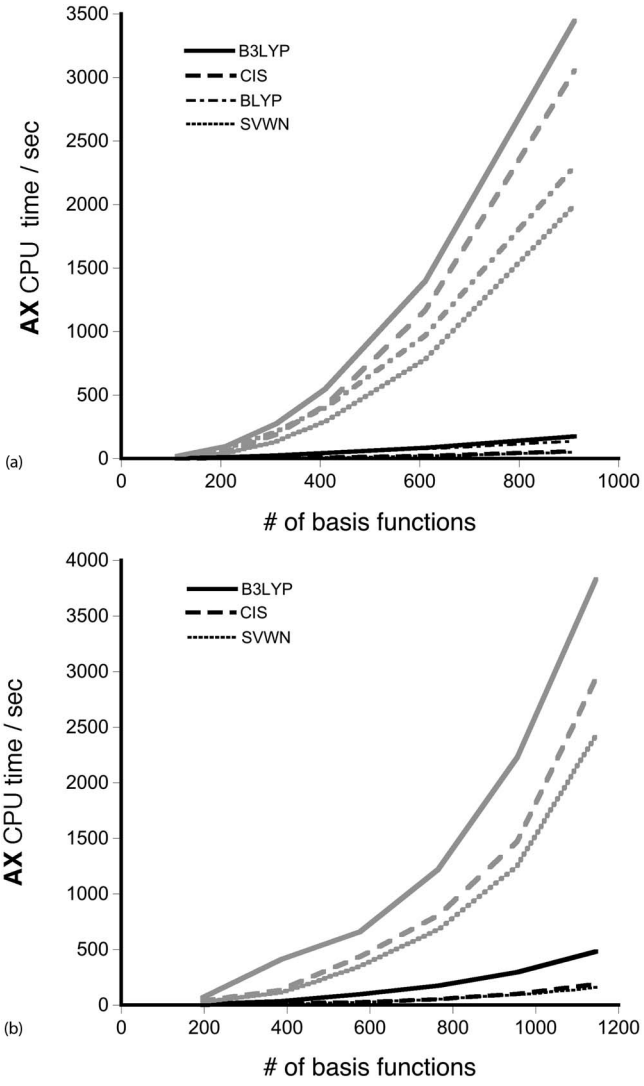

FIG. 3. CPU times per iteration for pseudospectral (black lines) and spectral (grey lines) TDDFT calculations on (a) polyenes and (b) microsolvated clusters of the PYP chromophore.

CONCLUSIONS

We have implemented the pseudospectral approximation for two-electron integral evaluation within the CIS and TDA-TDDFT methods. We have shown that PS-TDDFT reproduces conventional TDDFT excitation energies and oscillator strengths with significant reductions in computational complexity. The numerical results obtained suggest that the current implementation of PS-TDDFT should be useful in calculating the low-lying valence excited states in large-scale molecular systems.

In addition to the computational savings from the pseudospectral approach for the Coulomb and exchange integrals, we have found that extremely sparse grids may be used in the integration of the exchange-correlation functional for TDDFT. This leads to further reduction of computational cost without significant loss of accuracy in vertical excitation energies. This point is expected to be quite general and independent of the method used to evaluate the Coulomb and exchange integrals. This suggests that it would be fruitful to optimize grids specifically for the K_{xc} contribution in TDDFT, in contrast to the usual practice of using the same integration grids for K_{xc} in the KS-DFT and TDDFT stages of the calculation.

Of course, the use of the pseudospectral approximation in TDDFT cannot address the fundamental problems arising from incomplete knowledge of the exchange-correlation functional or those associated with the linear response and adiabatic approximations. Nevertheless, the present work makes TDDFT calculations significantly more efficient and moves the computational bottleneck from determination of excited state energies with TDDFT to the KS-DFT ground state calculation. In fact, the PS-TDDFT calculation itself is usually less costly than the ground state KS-DFT calculation for the test cases we have shown here.

ACKNOWLEDGMENTS

The authors are pleased to acknowledge many informative discussions about TDDFT with Professors R. M. Martin, K. Burke, R. Cave, and M. Casida. This work was supported by the National Science Foundation (DMR-03-25939 and CHE-07-19291), with additional support through the Frederick Seitz Materials Research Laboratory (DOE DEFG02-91ER45439).

[1] R. G. Parr and W. Yang, *Density-Functional Theory of Atoms and Molecules* (Oxford University Press, New York, 1989).
[2] M. E. Casida, in *Recent Advances in Density Functional Methods*, edited by D. P. Chong (World Scientific, Singapore, 1995), Vol. 1, p. 155.
[3] M. A. L. Marques and E. K. U. Gross, Annu. Rev. Phys. Chem. **55**, 427 (2004).
[4] H. Appel, E. K. U. Gross, and K. Burke, Phys. Rev. Lett. **90**, 043005 (2003).
[5] T. Grabo, M. Petersilka, and E. K. U. Gross, J. Mol. Struct.: THEOCHEM **501**, 353 (2000).
[6] E. Runge and E. K. U. Gross, Phys. Rev. Lett. **52**, 997 (1984).
[7] J. B. Foresman, M. Head–Gordon, J. A. Pople, and M. J. Frisch, J. Phys. Chem. **96**, 135 (1992).
[8] A. Dreuw and M. Head–Gordon, Chem. Rev. (Washington, D.C.) **105**, 4009 (2005).
[9] M. E. Casida, C. Jamorski, K. C. Casida, and D. R. Salahub, J. Chem. Phys. **108**, 4439 (1998).
[10] A. Dreuw, J. L. Weisman, and M. Head–Gordon, J. Chem. Phys. **119**, 2943 (2003).
[11] R. J. Cave, F. Zhang, N. T. Maitra, and K. Burke, Chem. Phys. Lett. **389**, 39 (2004).
[12] N. T. Maitra, F. Zhang, R. J. Cave, and K. Burke, J. Chem. Phys. **120**, 5932 (2004).
[13] B. G. Levine, C. Ko, J. Quenneville, and T. J. Martinez, Mol. Phys. **104**, 1053 (2006).
[14] C.-P. Hsu, S. Hirata, and M. Head–Gordon, J. Phys. Chem. A **105**, 451 (2001).
[15] B. O. Roos, Acc. Chem. Res. **32**, 137 (1999).
[16] R. A. Friesner, Annu. Rev. Phys. Chem. **42**, 341 (1991).
[17] T. J. Martinez and E. A. Carter, J. Chem. Phys. **98**, 7081 (1993).
[18] T. J. Martinez and E. A. Carter, J. Chem. Phys. **100**, 3631 (1994).
[19] T. J. Martinez, A. Mehta, and E. A. Carter, J. Chem. Phys. **97**, 1876 (1992).
[20] T. J. Martinez and E. A. Carter, in *Modern Electronic Structure Theory*, edited by D. R. Yarkony (World Scientific, Singapore, 1995), Vol. 2, p. 1132.
[21] T. J. Martinez and E. A. Carter, J. Chem. Phys. **102**, 7564 (1995).
[22] R. B. Murphy, Y. Cao, M. D. Beachy, M. N. Ringnalda, and R. A. Friesner, J. Chem. Phys. **112**, 10131 (2000).
[23] R. A. Friesner, R. B. Murphy, M. D. Beachy, M. N. Ringnalda, W. T. Pollard, B. D. Dunietz, and Y. Cao, J. Phys. Chem. A **103**, 1913 (1999).
[24] R. A. Friesner and B. D. Dunietz, Acc. Chem. Res. **34**, 351 (2001).
[25] R. A. Friesner, J. Chem. Phys. **85**, 1462 (1986).
[26] S. Hirata, M. Head–Gordon, and R. J. Bartlett, J. Chem. Phys. **111**,

10774 (1999).
[27] A. Szabo and N. Ostlund, *Modern Quantum Chemistry* (Dover, New York, 1996).
[28] S. Hirata and M. Head–Gordon, Chem. Phys. Lett. **314**, 291 (1999).
[29] N. H. F. Beebe and J. Linderberg, Int. J. Quantum Chem. **12**, 683 (1977).
[30] C. Van Alsenoy, J. Comput. Chem. **9**, 620 (1988).
[31] O. Vahtras, J. Almlof, and M. W. Feyereisen, Chem. Phys. Lett. **213**, 514 (1993).
[32] M. Sierka, A. Hogekamp, and R. Ahlrichs, J. Chem. Phys. **118**, 9136 (2003).
[33] Y. Jung, A. Sodt, P. M. W. Gill, and M. Head–Gordon, Proc. Natl. Acad. Sci. U.S.A. **102**, 6692 (2005).
[34] R. A. Kendall and H. A. Fruchtl, Theor. Chim. Acta **97**, 158 (1997).
[35] F. Aquilante, T. B. Pedersen, and R. Lindh, J. Chem. Phys. **126**, 194106 (2007).
[36] W. H. Press, S. A. Teukolsky, W. T. Vetterling, and B. P. Flannery, *Numerical Recipes in Fortran 77* (Cambridge University Press, Cambridge, 1992).
[37] D. Rappoport and F. Furche, J. Chem. Phys. **122**, 064105 (2005).
[38] A. D. Becke, J. Chem. Phys. **98**, 5648 (1993).
[39] Y. Tawada, T. Tsuneda, S. Yanagisawa, T. Yanai, and K. Hirao, J. Chem. Phys. **120**, 8425 (2004).
[40] B. Walker, A. M. Saitta, R. Gebauer, and S. Baroni, Phys. Rev. Lett. **96**, 113001 (2006).
[41] X. Andrade, S. Botti, M. A. L. Marques, and A. Rubio, J. Chem. Phys. **126**, 184106 (2007).
[42] S. Baroni, S. de Gironcoli, A. Dal Corso, and P. Gianozzi, Rev. Mod. Phys. **73**, 515 (2001).
[43] B. Roos, Chem. Phys. Lett. **15**, 153 (1972).
[44] M. N. Ringnalda, Y. Won, and R. A. Friesner, J. Chem. Phys. **92**, 1163 (1990).
[45] E. R. Davidson, J. Comput. Phys. **17**, 87 (1975).
[46] R. A. Friesner, J. Phys. Chem. **92**, 3091 (1988).
[47] R. A. Friesner, J. Chem. Phys. **86**, 3522 (1987).
[48] A. H. Stroud, *Approximate Calculation of Multiple Integrals* (Prentice-Hall, New York, 1971).
[49] V. I. Lebedev, Zh. Vychisl. Mat. Mat. Fiz. **15**, 48 (1975).
[50] B. H. Greeley, T. V. Russo, D. T. Mainz, J. Langlois, W. A. Goddard III, R. E. Donnelly, and M. N. Ringnalda, J. Chem. Phys. **101**, 4028 (1994).
[51] M. E. Mura and P. J. Knowles, J. Chem. Phys. **104**, 9848 (1996).
[52] J. M. Perez–Jorda, A. D. Becke, and E. San–Fabian, J. Chem. Phys. **100**, 6520 (1994).
[53] J. Baker, J. Andzelm, A. Scheiner, and B. Delley, J. Chem. Phys. **101**, 8894 (1994).
[54] A. D. Becke, J. Chem. Phys. **88**, 2547 (1988).
[55] JAGUAR v6.1, Schrodinger, LLC, New York, 2005.
[56] J. Lee, in *Chemi- and Bioluminescence*, edited by J. G. Burr (Marcel-Dekker, New York, 1985).
[57] M. A. van der Horst and K. J. Hellingwerf, Acc. Chem. Res. **37**, 13 (2004).
[58] J. J. P. Stewart, J. Comput. Chem. **10**, 209 (1989).
[59] L. X. Dang and B. M. Pettitt, J. Phys. Chem. **91**, 3349 (1987).
[60] J. J. P. Stewart, MOPAC 2000, Fujitsu Limited, Tokyo, Japan, 1999.
[61] J. Almlof, K. J. Faegri, and K. Korsell, J. Comput. Chem. **3**, 385 (1982).
[62] Selection of these grids for Coulomb/exchange evaluation within JAGUAR is performed by setting the keyword iopt287 to 1, 2, 12, or 9 for the c, m, C, and M grids, respectively. Similarly, the keyword iopt286 can be set to the same values to select the grid which is used for the quadrature of the exchange-correlation contribution.
[63] Y. Shao, L. Fusti–Molnar, Y. Jung *et al.*, Phys. Chem. Chem. Phys. **8**, 3172 (2006).
[64] J. C. Slater, *The Self-Consistent Field for Molecules and Solids* (McGraw-Hill, New York, 1974).
[65] S. H. Vosko, L. Wilk, and M. Nusair, Can. J. Phys. **58**, 1200 (1980).
[66] A. D. Becke, Phys. Rev. A **38**, 3098 (1988).
[67] C. Lee, W. Yang, and R. G. Parr, Phys. Rev. B **37**, 785 (1988).
[68] Y. Zhao and D. G. Truhlar, J. Phys. Chem. A **110**, 13126 (2006).